Atmos. Meas. Tech. Discuss., https://doi.org/10.5194/amt-2017-301
Manuscript under review for journal Atmos. Meas. Tech.
Discussion started: 22 August 2017

Atmospheric Measurement Techniques
Discussions

Retrieval of ozone profiles from OMPS limb scattering observations

Carlo Arosio[1], Alexei Rozanov[1], Elizaveta Malinina[1], Kai-Uwe Eichmann[1], Thomas von Clarmann[2], and John P. Burrows[1]

[1]Insitute of Environmental Physics, University of Bremen, Bremen, Germany
[2]Karlsruhe Institute of Technology, Karlsruhe, Germany

Correspondence to: carloarosio@iup.physik.uni-bremen.de

Abstract. This study describes a retrieval algorithm developed at the University of Bremen to retrieve vertical profiles of ozone from limb observations performed by the Ozone Mapper and Profiler Suite (OMPS). This algorithm was originally developed for use with data from the SCIAMACHY instrument. As both instruments make limb measurements of the scattered solar radiation in the ultraviolet and visible spectral range, an overarching objective of the study is to facilitate the provision of consolidated and consistent ozone profiles from the two satellites and to produce a combined data set. The optimization of the retrieval algorithm for OMPS takes into account the instrument-specific spectral coverage by exploiting information from spectral windows in the Hartley, Huggins and Chappuis ozone absorption bands. Thereby, ozone concentrations in the 12 - 60 km altitude range can be retrieved. Observations at altitudes where the measurements are contaminated by clouds are rejected by applying a cloud filter. An independent aerosol retrieval is performed beforehand and its results are used to account for the aerosol load in the stratosphere during the ozone retrieval. Results for seven months of data (July 2016 - January 2017) are compared and validated against independent data sets from both satellite-based and balloon-borne measurements, indicating a good agreement. Between 20 and 50 km, the OMPS ozone profiles typically agree with the MLS v4.2 results within 5-10 %, with the exception of high northern latitudes (> 70° N above 40 km) and the tropical lower stratosphere. The comparison of OMPS profiles with those from ozonesondes shows an agreement within ±5 % between 14 and 30 km at northern mid-latitudes. At southern mid-latitudes, an agreement within 5-10 % is achieved, although these results are less reliable because of a limited number of available coincidences. An unexpected bias of approximately 10 % is detected in the tropical region at all altitudes. The processing of the 2013 data set using the same retrieval settings and its validation against ozonesondes reveals a much smaller bias; possible reasons are under investigation.

1 Introduction

Ozone is one of the most important trace gases in the atmosphere. This is due to its stratospheric layer, which absorbs strong ultraviolet (UV) radiation heating this atmospheric region and thereby acting as a protective layer against biologically harmful radiation. It is relevant to climate because of its crucial role in the radiative budget of the stratosphere. The presence of a stratospheric ozone layer was first discussed by Hartley (1880) but came to prominence in the late 1960s and early 1970s when it was first recognized that anthropogenic activities could result in the depletion of stratospheric and mesospheric ozone (Molina and Rowland, 1974). Ozone is also of importance in the tropospheric chemistry and it is a greenhouse gas, thus its amount and spatial distribution play a role in the global warming and climate change processes (IPCC 5th report, Pachauri and Meyer (2014)).

After the recognition that man made release of chlorofluorocarbon compounds depletes the stratospheric ozone layer and the discovery of the springtime ozone hole in Antarctica (Farman et al., 1985), the field of stratospheric chemistry and physics researches expanded. This resulted in the mechanism of the production and loss of stratospheric ozone being much better explained. Although nowadays the stratospheric ozone chemistry is generally well understood, there are still several issues to be clarified. These are related to the expected ozone recovery after the Montreal protocol adoption, long term ozone trends and stratospheric responses to changes in tropospheric radiative fluxes and temperatures. For example, Solomon et al. (2016) focused the attention on the Antarctic region, investigating possible signatures of an ozone healing. Analyzing observations collected each September since 2000, the authors suggested that the fingerprints of an ozone recovery can be identified in both the increase of its column amount and in the decrease of the areal extent of the ozone hole.

The issues related to changes in the Brewer Dobson Circulation (BDC), possibly linked to climate changes, are investigated by several studies, that consider the ozone concentration in the lower stratosphere a good proxy to track changes in the stratospheric circulation. Among them, Aschmann et al. (2014) used combined O_3 time series from satellite instruments and ozonesondes to investigate changes in the BDC after the beginning of the century and identified an asymmetry in the BDC northern and southern branches. Stiller et al. (2017) suggested a shift of the subtropical mixing barriers as an explanation of this asymmetry. Recent attempts to consistently merge a large number of different data sets to study trends are reported by Steinbrecht et al. (2017) and Sofieva et al. (2017), revealing a global statistically significant increase in the ozone amount after 2000 above 35 km. Other authors, as Kyrölä et al. (2013), Eckert et al. (2014), Gebhardt et al. (2014) and Nedoluha et al. (2015) pointed out an unexpected decadal negative trend in the ozone abundance in the upper tropical stratosphere.

The occurrence of strong ozone loss events over the Arctic during spring after particularly cold stratospheric conditions, as occurred in 2011 and 2016, drew the attention of scientists and public concern to the possible consequences for human health (Manney et al., 2011). Current predictions of a long term impact of global warming coupled with the removal of ozone depleting species indicate a colder stratosphere and an increase in stratospheric ozone, a so-called super recovery of ozone (WMO (2014)). For all these kinds of studies, reliable long-term data sets are needed both from ground-based instruments and satellite observations: for example, recent discussions have shown the importance of multi-decadal time series in order to detect trends in the ozone concentration and the possible recovery of the ozone layer in the Antarctic region (Stolarski and Frith, 2006)

During the last few decades, several remote sensing observation techniques have been used to derive ozone concentrations from the troposphere up to the mesosphere (Hassler et al., 2014). Following the birth of the space age, instrumentation of different kinds began to be developed. Space-borne remote sensing measurements in the Ultraviolet-Visible (UV-VIS) spectral range have traditionally been of two types: nadir viewing and solar occultation spectrometers; the former instruments point downward while the latter look directly into the solar disk. A more recent technique, the limb scatter of sunlight, combines the advantages of the other two techniques and provides vertical profiles of ozone density with relatively high vertical resolution and horizontal coverage. The same geometry of observation can also be exploited to collect measurements in the InfraRed (IR) or microwave spectral regions, the so called limb emission measurements. With this latter technique a day and night coverage of the globe is feasible.

One of the instruments capable of performing limb-scatter observations in the UV, VIS, Near InfraRed (NIR) and Short Wave InfraRed (SWIR) spectral ranges was the SCanning Imaging Absorption spectroMeter for Atmospheric CHartographY (SCIAMACHY), launched in March 2002 (Burrows et al. (1995), Gottwald and Bovensmann (2011)). In early 2012 ground communication with the European Space Agency ENVISAT satellite, carrying SCIAMACHY among other ozone science relevant instruments, was lost. A few aging satellite missions, such as the Optical Spectrograph and InfraRed Imager System (OSIRIS) and the Microwave Limb Sounder (MLS), are still operating, contributing to the task of continuous monitoring the stratospheric ozone. At the end of 2011, just a few months before the end of ENVISAT lifetime, the Ozone Mapping and Profiler Suite (OMPS) instrument was launched and it is still operational (Flynn et al., 2014).

In this paper the retrieval algorithm developed at the University of Bremen to retrieve vertical ozone profiles from OMPS limb observations is discussed. An overarching objective for the study is the creation of a consolidated data set and the merging of the OMPS and the SCIAMACHY time series, in order to obtain a long-term continuous data set. For a description of SCIAMACHY v3.0 ozone retrievals refer to Jia et al. (2015). In Sect. 2 of this paper, the OMPS instrument is introduced: its geometry of observation, relevant characteristics and issues related to the retrieval of ozone are briefly discussed. The third section is focused on the retrieval methodology, starting with a general description of the inversion algorithm used in this work. A more detailed characterization of the retrieval procedure follows, including the applied cloud filter, the retrieval of aerosol extinction profiles and of the surface albedo. In Sect. 4, first a comparison with NASA ozone profile retrieval algorithm is shown; then MLS and ozonesonde data sets are used for a first validation of our results. Main results, remaining issues and possible future improvements are addressed in the latter section and in the conclusions.

2 OMPS-LP Instrument

2.1 General features

The Suomi-National Polar-Orbiting Operational Environmental Satellite System Preparatory Project (SNPP) platform carrying the OMPS instrument was launched in October 2011 and OMPS data collection started in January 2012. The spacecraft has a nominal 13:30 local time ascending sun-synchronous orbit and flies at a mean altitude of 833 km. The main objective of the mission is to monitor the ozone vertical distribution within the Earth middle atmosphere at high accuracy level. OMPS comprises three instruments: a Nadir Mapper, a Nadir Profiler and a Limb Profiler (LP). Only the latter is of interest for our study (see Flynn et al. (2014) for a review of the full suite). OMPS-LP images the Earth atmosphere by viewing its edge (limb) from space. The closest approach of the sensor line of sight to the Earth surface is referred to as the Tangent Point (TP) and the altitude of this point above the Earth geoid is called Tangent Height (TH); the limb geometry is schematically drawn in Fig. 1.

The OMPS-LP sensor views at the Earth limb backwards with respect to the flying direction, through three vertical slits: the central one is aligned along the nadir track, while the other two are cross-track, separated horizontally by 4.25°, which corresponds to 250 km distance between the TPs. Each slit covers a vertical range of 112 km, imaging the atmosphere without

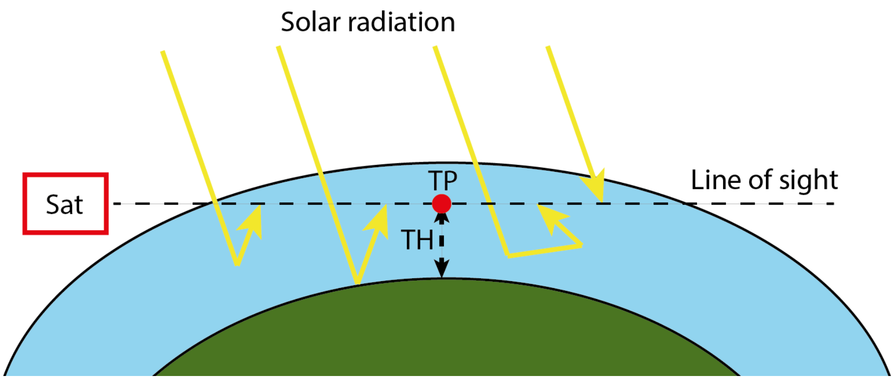

Figure 1. Schematic diagram of the viewing geometry of a satellite limb observation

scanning. OMPS-LP was designed to measure ozone vertical distributions in the upper troposphere and stratosphere with an instantaneous field of view of about 1.5 km and a sampling of 1 km at TP (Jaross et al., 2014). The orbit is inclined, so that the TP is located on the East with respect to the satellite, around 25° latitude South of the sub-satellite point. The geometry is drawn in Fig. 2. OMPS-LP performs normally 180 limb observations (referred to as states) per orbit, around 160 of which with solar zenith angle less then 80°, and completes 14-15 orbits per day.

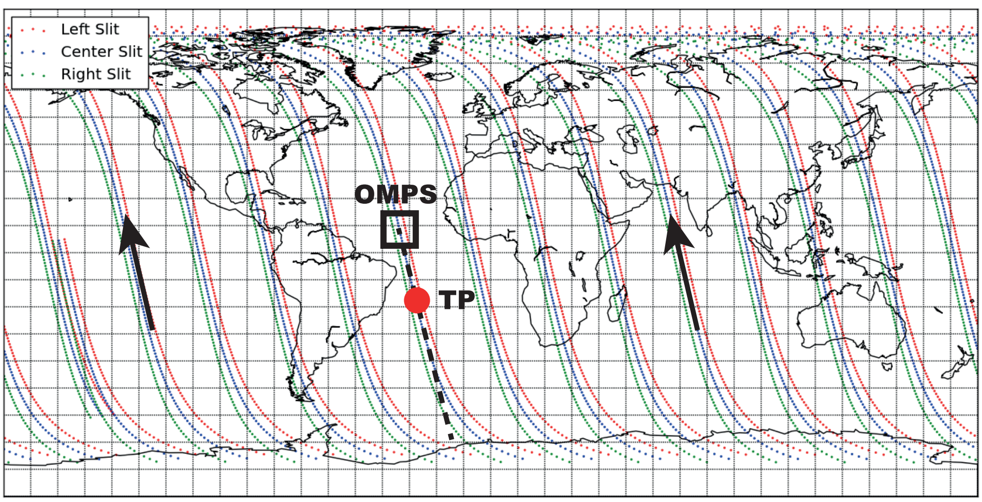

Figure 2. OMPS daily orbits and observation geometry sketch; black arrows indicate the satellite flight direction. Adapted from Bhartia et al. (2013)

The instrument measures limb-scatter radiance in the spectral range between 280 nm and 1000 nm. A particular characteristic of this instrument is the use of a prism spectrometer instead of a grating disperser. The employed prism provides a spectral resolution that degrades with the wavelength, from 1 nm in the UV region up to 40 nm in the NIR. The full atmospheric range is observed at the same time, without vertical scanning, and radiance is collected by means of Charge-Coupled Devices (CCD). The use of such a technology poses a great challenge as regards the Signal to Noise Ratio (SNR): indeed, scattered solar radiance from the Earth limb decreases by at least five orders of magnitude along the considered vertical range, due to the decrease of atmospheric density. So, in order to cover the required dynamic range, four images at two physical CCDs are taken for each slit: the full atmosphere is imaged at two integration times (that differ by a factor 30) and through a large and a small aperture (Jaross et al., 2014). Then, since the down-link rate is by far slower that the data collection rate, only a selected number of pixels from these four images can be transferred. Ground processing is needed to select unsaturated signals and combine down-linked pixels from different images in a single radiance file. The combined image features a non-uniform wavelength and TH grid (spectral and vertical smile), so it is re-sampled and mapped onto a regular grid. Example of radiance profiles that show the large dynamic range of measured values are shown in Fig. 3. The gridding procedure is performed using a bi-linear interpolation and pixel-to-pixel calibration errors linked to this consolidation procedure are estimated to be around 1 %. As radiance measured at large and small aperture can differ by several percents, radiance profiles at a specific wavelength are derived from one aperture only; on the contrary, a better consistency is found between long and short integration time, so that they are combined at different altitudes to get each radiance profile. Jumps in the SNR plot (Fig. 4) are related to changes of the sampled image: for example, the jump between large and small aperture that occur at 450 nm (fixed threshold). In the retrieval scheme we were careful not to consider spectral ranges crossing this fixed boundary.

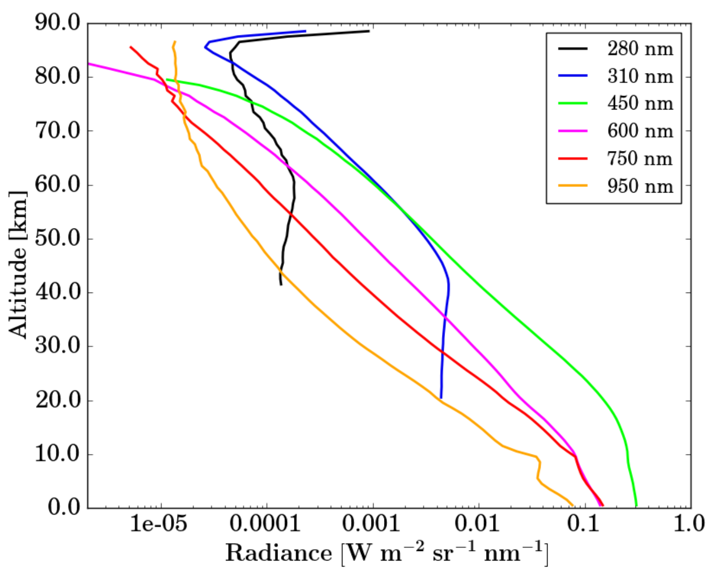

Figure 3. Example of OMPS-LP radiance profiles at some wavelengths.

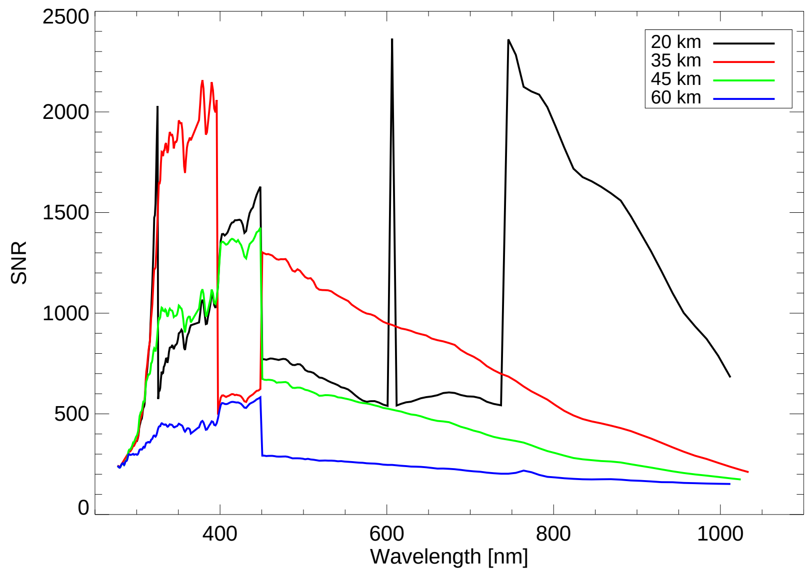

Figure 4. Example of OMPS-LP SNR at different tangent heights.

2.2 Calibration and main issues

Level 1 (L1) data used in this study are provided by NASA team (Jaross et al., 2014) and used without any further prior handling. One of the most important issues that affects the quality of the limb scattering technique is the TH registration. In order to retrieve reliable ozone profiles, the TP altitude has to be known with high precision: in fact, a 200 m uncertainty in the TP height translates into a 5 % error in the ozone profile. Such a high accuracy can not be directly reached for OMPS-LP sensor. This is because the star-tracker on board the SNPP satellite is mounted on a distant position from the instrument, so that thermal effects and errors in the instrument focal plane alignment increase the uncertainty. To solve this problem, a technique called Rayleigh Scattering Altitude Sensing (RSAS) is implemented by the NASA team in the L1 data processing (Moy et al., 2017). This technique exploits the fact that at 350 nm the atmosphere at low altitudes becomes opaque enough not to let the TP be seen; on the contrary, above 30 km limb scattered radiation decreases accordingly with the atmospheric density. So, a comparison between measured and simulated 30 km/20 km radiance ratio yields an estimate of the applicable tangent altitude correction. Averaged values of the TH corrections span between 1 and 2 km (respectively for the east and west slits), meaning that the instrument points at altitudes higher than expected. Fixed adjustments are applied independently for each slit.

Another issue that was discovered after the satellite launch concerns the thermal drift of the instrument: during each orbit, as it approaches northern mid-latitudes, sunlight directly hits the limb sensor causing its rapid heating up. As a consequence, both spectral and spatial shifts occur, affecting the three slits in different ways. The related average TH variation is on the order of 500 m and fixed but latitudinal dependent corrections are actually applied for every orbit; the largest uncertainty of this correction is at northern latitudes, where the solar heating is the greatest. In addition, a further dynamic TH variation within each orbit has been detected: intra-orbital TH error varies almost linearly with latitude. The current estimate is around 400 m change from the South to the North Pole, but a satisfactory explanation for this variation still has to be found. Currently, this effect is not corrected for. Finally, long-term drifts and seasonal variations in pointing with a magnitude of 200 m have been detected using RSAS results and another scene-based technique. These may also result from errors in the used temperature profile and are not currently corrected.

The second important issue that affects the accuracy of limb radiance is the so-called stray light. The general phenomenon of stray light describes photons that are registered by the detector at wavelengths or altitudes which they do not belong to. There are several causes of stray light. For example, as limb scattering is proportional to air density, photons from lower altitudes can be scattered within the instrument to detector areas associated with different altitudes or wavelengths. Furthermore, with multiple images on a single detector, photons from the IR part of one slit can be scattered into the UV part of the neighboring image. This problem was reduced with both a thorough study of the point spread function during the pre-launch operations and with the careful application of cutoff filters at the focal plane (Jaross et al., 2014). The full detector response to several point sources was extensively studied during ground testing: a stray light matrix was created, providing the basis for subtracting the stray light contribution from the measured Earth limb radiance. Stray light is mainly an issue at high altitudes, with levels that are usually less then 10 % of the measured value and tend to increase with altitude for the same wavelength.

The CCD used for detection of photons for OMPS-LP operates at -45 °C to minimize dark current and other noise sources. Dark current and non-linearity of the sensor are corrected accurately and introduce minor errors in the reported radiance. The instrument uses a diffuser in the field of view in order to measure the extraterrestrial solar spectrum and maintain the spectral registration. Transient events can affect the instrument reliability: energetic charged particle can penetrate through the CCD shielding and cause transients in pixel signal. Such events are frequent in the so called South Atlantic Anomaly. A related quality flag is reported in L1 data and used in this study for the comparison with NASA retrieval (Kahn and Kowitt, 2015).

In this paper version 2.5 of OMPS-LP L1 gridded data has been used; the treatment of stray light has been improved with respect to the previous version and the RSAS technique for pointing corrections fully implemented (corrections were discussed above). In addition, both sun-normalized and absolute radiances are provided. In the preparation time of this paper the new data version was not fully released and only seven consecutive months were available, from July 1, 2016 till January 31, 2017. Retrievals were performed using data from the central slit of the instrument only because the lateral slits can still suffer from pointing issues.

2.3 OMPS-LP geometry of observations

Several angular coordinates are needed in the retrieval algorithm to correctly describe the observation geometry; satellite azimuth (φ), solar azimuth (φ_0) and solar zenith angle (ψ_0) at the TP are reported for three THs (25, 35 and 45 km) in the L1 data files and are used to define the geometry of the observation. The solar zenith angle (ψ_0) is defined as the angle between the local vertical at the TP and the sun pointing vector. The azimuth angles (φ and φ_0) are defined as the angles between the direction to the North Pole and projections of the solar beam and the instrument line of sight, respectively, on the plane orthogonal to the normal vector at the TP; by convention, positive angles are East of the North, so that values are inside the [-180, 180]° range. Looking at the OMPS-LP observation geometry and considering only solar zenith angles less than 80° to avoid high stray light levels, the satellite azimuth angle is always negative while the solar azimuth angle changes sign along the orbit.

Combining solar azimuth and zenith angles, the scattering angle θ at the TP can be computed as:

$$\cos(\theta) = \sin(\psi_0)\cos(\varphi - \varphi_0) \tag{1}$$

This is an important quantity that defines the scattering geometry. In Fig. 5 values of scattering angles together with solar zenith angles are plotted as a function of latitude for three OMPS orbits in different seasons. The solar zenith angles are shown as solid lines, with symmetric values with respect to the equatorial region; scattering angles are plotted as dashed lines.

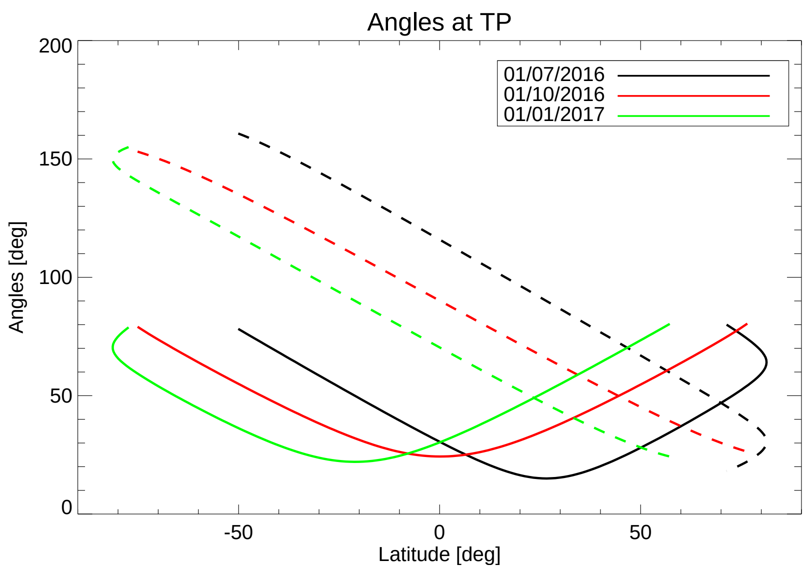

Figure 5. Solar zenith angles (solid lines) and scattering angles (dashed lines) at the TP along three OMPS orbits on the following dates: Jul 1 2016, Oct 1 2016 and Jan 1 2017.

3 Retrieval method

3.1 The retrieval algorithm

The retrieval is done using the regularized inversion technique with the first order Tikhonov constraints (Tikhonov (1963), Rodgers (2000)). A non-linearity of the inverse problem is accounted for using an iterative approach. The forward modeling is performed taking into consideration atmospheric multiple scattering in the framework of the approximate spherical mode of the SCIATRAN radiative transfer model (Rozanov et al., 2014). The CDI (Combined Differential-Integral) model is employed to solve the radiative transfer equation: first, the entire radiation field is calculated in the pseudo-spherical approximation for a set of solar zenith angles using the finite difference method. Then, an integration along the line-of-sight is carried out calculating the single scattering contribution in a fully spherical geometry and using the pseudo-spherical radiation field to account for the multiple scattering contribution (Rozanov et al., 2000). The integration along the line-of-sight is performed accounting also for the atmospheric refraction. The weighting functions are calculated using the same method as for the radiance, but in this case the single scattering contribution only is considered.

For the OMPS-LP retrieval, four spectral segments are selected: three in the UV spectral region (Hartley and Huggins bands) and one in the visible Chappuis band; the former ranges are sensitive to upper stratospheric ozone, while the latter to the lower stratospheric region, where the peak of the number density occurs. Details are listed in Table 1. The altitude range over which the retrieval is performed spans between 12 and 60 km above the sea level. Limb radiance in each spectral interval is first normalized with respect to a limb measurement at an upper TH, in order to provide a self calibration of the instrument and reduce the effect of surface/cloud reflectance. In addition, a polynomial is subtracted from the logarithm of the normalized radiance in the visible range in order to get rid of slowly-variable spectral features, e.g. caused by aerosol scattering (Rozanov et al., 2011).

Table 1. List of the spectral segments considered in the ozone retrieval with respective altitude ranges and THs used for the normalization.

Altitude range [km]	Spectral segment [nm]	TH normalization [km]
46-60	285-300	63
35-46	305-313	52
31-36	322-331	47
12-33	508-660 †	42

† 580.0 - 607.0 and 620.0 - 635.0 nm ranges are rejected.

In the forward model, the following molecular species with spectral signatures in the selected spectral ranges are considered: O_3, NO_2 and O_4. Cross sections of these gases are respectively taken from Serdyuchenko et al. (2014), Bogumil et al. (2000) and Hermans (2011). Cross sections are beforehand convolved to the OMPS-LP spectral resolution. In order to avoid absorption lines of water vapor and of O_2, wavelengths between 580.0 and 607.0 and between 620.0 and 635.0 are rejected. A complete treatment of these absorption features requires line-by-line calculations, that are computationally expensive. Ancillary pressure and temperature profiles used in the radiative transfer model are taken from the Global Modeling and Assimilation Office (GMAO) interpolated data set, provided by the NASA team together with OMPS-LP L1 radiances.

At a pre-processing step, a shift and squeeze correction is applied in the Chappuis band to the modeled spectrum with respect to the measured one; this pre-processing is performed for each observation at each TH independently. Typical values for the spectral shift are inside the range [+1,+4] nm for the first point of the interval and [-2,+1] nm for the last spectral point. In the UV range no shift and squeeze correction is applied.

Linearizing the forward model around an initial guess state $\boldsymbol{x_0}$, the general equation that has to be solved can be written as:

$$\boldsymbol{y} = \boldsymbol{y_0} + \mathbf{K}(\boldsymbol{x} - \boldsymbol{x_0}) + \boldsymbol{\epsilon} \tag{2}$$

where $\boldsymbol{y}$ is the measurement vector, $\boldsymbol{y_0}$ is the simulated spectrum, $\mathbf{K}$ is the linearized forward model operator represented by the weighting function matrix, $\boldsymbol{x}$ is the state vector containing the retrieved ozone vertical distributions in terms of Volume Mixing Ratio (VMR), and ϵ represents errors of any kind.

Following (Rodgers, 2000), the solution of Eq. (2) can be estimated iteratively. Taking into consideration that in our algorithm the retrieval is performed from a zero a priori profile, the iterative step $i+1$ can be expressed as:

$$\boldsymbol{x_{i+1}} = (\mathbf{K_i^T S_\epsilon}^{-1}\mathbf{K_i} + \mathbf{S_0} + \gamma \mathbf{S_1^T S_1})^{-1}\mathbf{K_i^T S_\epsilon}^{-1}(\boldsymbol{y} - \boldsymbol{y_i} + \mathbf{K_i}\boldsymbol{x_i}) \tag{3}$$

Here, $\mathbf{S}_\epsilon$ is the measurement noise covariance matrix. It is obtained from the fit residuals after the pre-processing procedure, assuming that absorption features from gases other than O_3 in the selected windows are negligible, while O_3 is fitted. $\mathbf{S_0}$ is the diagonal matrix optimized to constrain the solution within physically meaningful values and minimize the possible negative bias caused by the use of a zero a priori profile. The effect of the chosen matrix is significant only at tropical low altitudes and globally at high altitudes, where the ozone VMR is very small. Finally, $\mathbf{S_1}$ is the first order derivative matrix ($\mathbf{S_1^T S_1}$ is the first order Tikhonov term), weighted by a parameter γ that linearly increases with height above 45 km, used to constrain the smoothness of the retrieved profile. In Eq. (4), the sum $\mathbf{S_0} + \gamma \mathbf{S_1^T S_1}$ will be named as $\mathbf{S_r}$. The information content of the measurements as well as the sensitivity of the retrieval can be analyzed using the averaging kernels ($\mathbf{A}$) and the covariance of retrieval noise ($\mathbf{S_m}$) obtained respectively as (Rodgers, 2000):

$$\mathbf{A} = (\mathbf{K^T S_\epsilon}^{-1}\mathbf{K} + \mathbf{S_r})^{-1}\mathbf{K^T S_\epsilon}^{-1}\mathbf{K} \qquad \mathbf{S_m} = (\mathbf{K^T S_\epsilon}^{-1}\mathbf{K} + \mathbf{S_r})^{-1}\mathbf{K^T S_\epsilon}^{-1}\mathbf{K}(\mathbf{K^T S_\epsilon}^{-1}\mathbf{K} + \mathbf{S_r})^{-1} \tag{4}$$

The square root values of the diagonal elements of the retrieval noise covariance matrix $\mathbf{S_m}$ are commonly referred to as the theoretical precision of the retrieval. The vertical resolution of the retrieved profile is computed as the inverse of the diagonal elements of the averaging kernel matrix, scaled by the altitude grid width. Examples of averaging kernels, vertical resolution and theoretical relative precision are plotted in Fig. 6. One can notice that below 35 km the actual vertical resolution of the retrieval scheme is about 2-3 km with a peak around 35 km where the transition between UV and VIS spectral regions occurs. The relative uncertainty of the ozone profiles is in the range 1-5 % above 25 km and increases up to 10-20 % below 20 km.

Simultaneously with the ozone retrieval, surface albedo in UV and VIS spectral ranges is estimated exploiting the sun normalized product: the two spectral intervals between 355 and 365 nm and between 455 and 470 nm are used, where ozone absorption has a minimum, and three THs around 38 km are considered.

In order to tailor the retrieval scheme to OMPS-LP data, a three way approach is followed:

1. An evaluation of ozone weighting functions is performed. Each selected spectral interval contains information originating from a range of altitudes that could be estimated analyzing the ozone weighting functions. Each of these spectral segments is used at those THs where it provides most information on ozone VMR.

2. An analysis of spectral fits is carried out, to detect spectral ranges where the model fit is not satisfactory. During the test phase, spectral ranges are adjusted looking at fit residuals and at the structure of the retrieved profile: oscillations or unexpected jumps between different altitude regions are avoided.

Atmos. Meas. Tech. Discuss., https://doi.org/10.5194/amt-2017-301
Manuscript under review for journal Atmos. Meas. Tech.
Discussion started: 22 August 2017

Atmospheric Measurement Techniques Discussions

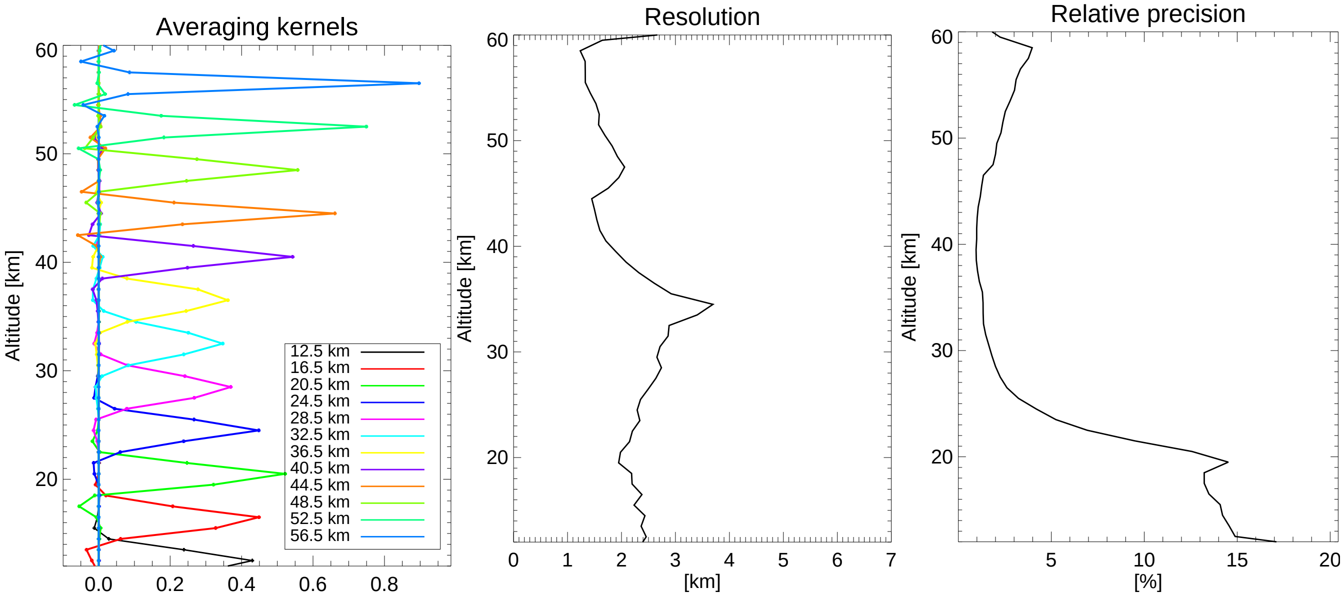

Figure 6. From left to right, examples of averaging kernels (plotted every 4 km for sake of clarity), vertical resolution and theoretical relative precision of the retrieval scheme, for a measurement at 30° N.

3. An evaluation of the averaging kernels is done. As we mentioned above, the worst values of the vertical resolution of the retrieval are found around 35 km, which is in the transition region between dominating contributions from VIS and UV ranges. The choice of the spectral interval for this altitude is aimed at optimizing the vertical resolution of the retrieval.

3.2 Cloud Filter

A cloud filter is applied during the ozone retrieval to reject THs affected by the presence of clouds. The applied algorithm is based on the Color Index Ratio (CIR) concept (Eichmann et al., 2016) using OMPS-LP radiance at 754 nm and 997 nm. The so-called Color Index (CI) is obtained calculating the ratio of the radiance at the two chosen wavelengths for the same OMPS-LP state. The CI is an altitude dependent quantity and can be used to detect the presence of scattering particles in the field of view, since we know the expected ratio for a cloud-free atmosphere. First, the CI is calculated at all THs, then the CIR is obtained as:

$$CIR(z_{th}) = \frac{CI(z_{th})}{CI(z_{th} + \Delta z_{th})} \tag{5}$$

An example of the results for simulated clouds is reported in Fig. 7: cirrus clouds consisting of hexagonal crystals with an optical depth between 0.01 and 0.15 are taken into consideration. Since the ozone retrieval is run above 12 km, we are generally not interested in water clouds.

The chosen threshold to flag a TH as cloudy is 1.25. This technique was also applied to SCIAMACHY measurements with a different threshold (Eichmann et al., 2016). At the considered wavelengths the measured radiation is related to the

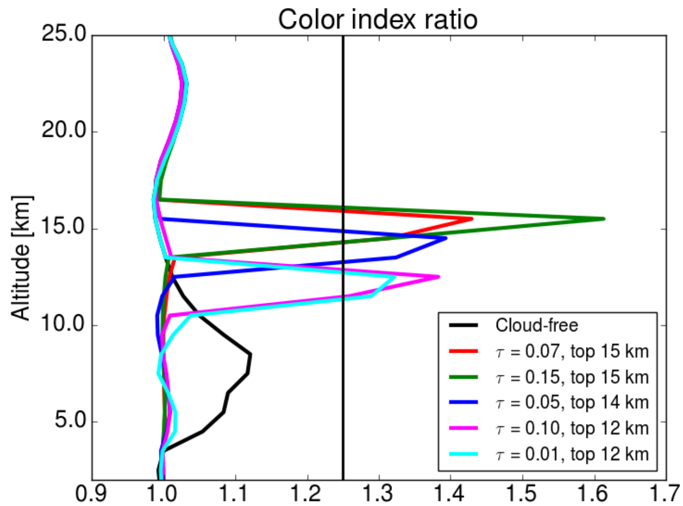

Figure 7. Example of Color Index Ratios for different simulations of ice clouds. Top of the cloud and optical depth (τ) ranges are chosen to simulate the impact of thin cirrus clouds in the upper troposphere.

scattered light from molecules, aerosol or cloud particles. A question may arise regarding the inability of such an approach to distinguish between high aerosol loads and cirrus clouds. Future investigations will focus on a comparison between the CIR filter and aerosol profiles retrieved as described in the next subsection.

3.3 Aerosol treatment

Aerosol extinction coefficient is retrieved employing the general approach as used for SCIAMACHY v1.4 stratospheric aerosol extinction product (Rieger et al., 2017). Since OMPS-LP has a coarser spectral resolution, the retrieval at 750 nm as used for SCIAMACHY is sub-optimal because of the influence of the O_2 absorption band. Instead, a wavelength of 868.8 nm is chosen. Stratospheric aerosol extinction is retrieved in the altitude range from 10.5 km to 33.5 km. The spectrum at 34.5 km is used as the reference; the Lambertian albedo is simultaneously retrieved using the sun-normalized spectrum at 34.5 km. In order to smooth spurious oscillations, the first order Tikhonov regularization is employed. Scattering phase functions are calculated using Mie scattering theory. Thereby, the particle size distribution is assumed to be lognormal with the median radius (r_g) of 0.08 μm, and distribution width parameter (σ) of 1.6. This distribution is described by the following equation:

$$n(r) = \frac{N}{\sqrt{2\pi}\ln(\sigma)r} \exp\left(\frac{(\ln(r_g) - \ln(r))^2}{2\ln^2(\sigma)}\right) \tag{6}$$

The aerosol particles are assumed to be sulfuric droplets with 0 % relative humidity in the surrounding atmosphere. Below 10 km and above 46 km the aerosol load is set to zero. The refractive indexes are calculated using the Optical Properties of Aerosols and Clouds (OPAC) database (Hess et al., 1998).

Before using the retrieved aerosol product, altitudes downwards from the detected cloud top height are rejected and each profile is extrapolated by the scaled a priori. The scaling factor is derived averaging three altitude levels above the cloud.

4 Satellite data set comparisons

4.1 NASA retrieval and comparison

To retrieve ozone profiles from OMPS-LP observations, the NASA team has implemented the Environmental Data Record algorithm that processes L1 together with the provided ancillary data: in this procedure, a series of secondary parameters such as surface albedo, cloud height and TH correction are derived before the main retrieval of ozone profiles (Rault and Loughman, 2013). Two spectral ranges are exploited for the latter task: UV wavelengths are used between 30 and 60 km, while the Chappuis band (520 and 650 nm) is used between 6 and 40 km (the bottom height depends on the detected cloud top altitude). The NASA retrieval algorithm is based on an inversion scheme with a priori constraints and a Tikhonov regularization. The normalization of the radiance is performed with respect to high altitude TH measurements: 65 km in UV and 45 km in VIS. The measurement vector is obtained using the doublet and triplet method respectively for the Hartley-Huggins and Chappuis bands; more details are given in Table 2. Comparison between NASA-OMPS retrieval and our results (in the following called IUP-OMPS) is reported in Fig. 8 for the tropical region. Only measurements at solar zenith angles less than 80° are compared to avoid stray light issues. At the moment of the submission of the paper, only version 2 of Level 2 (L2) NASA product was available, so a comparison with the most recent retrieval could not be performed.

Table 2. Wavelengths used in the NASA-OMPS ozone retrieval, according to Rault and Loughman (2013)

Parameters	Values
Doublet λ_0	355 nm
Triplet λ_l	500 nm
Triplet λ_r	680 nm
Wavelength used in UV (nm)	289.3 - 303.0; 308.9 - 311.6; 318.0-312.7
Wavelength used in VIS (nm)	522.8, 526.3, 549.9, 554.3, 572.1, 576.9, 602.5
	608.1, 613.4, 619.6, 624.8, 637.4, 643.4, 649.7

A direct comparison between NASA and IUP-OMPS retrieval products is reported in Fig. 8, showing relative differences for the tropical region, southern and northern mid-latitude bands. Differences are generally within ±10 % above 20 km; in the NASA product the peak values around 25 km are generally lower than in the IUP results in all the latitude bins. In the lower stratosphere we can also note a disagreement between the two profiles, with the IUP data showing lower values.

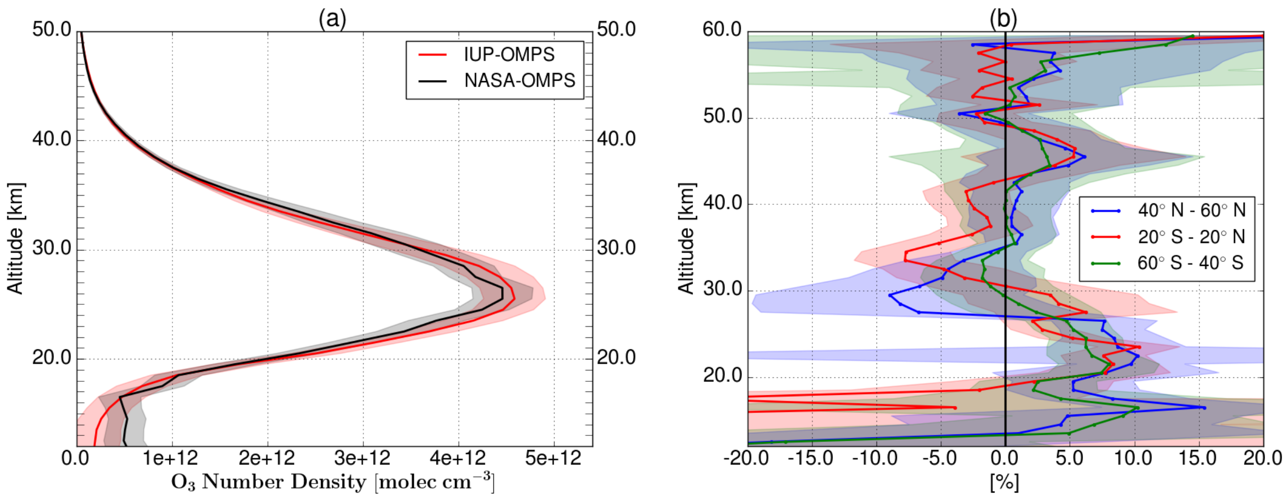

Figure 8. Panel (a): IUP-OMPS and NASA-OMPS retrieved number density profiles averaged in the tropical region. Panel (b): relative differences between IUP-OMPS and NASA-OMPS retrievals are shown in the three latitudinal bands 40° N - 60° N, 20° S - 20° N and 60° S - 40° S, with respective standard deviation as shaded area.

4.2 MLS comparison

The MLS instrument was launched on board the AURA satellite in July 2004 to observe the thermal emission from atmospheric trace gases in the millimeter/sub-millimeter spectral range. It scans the Earth limb 240 times per orbit, providing retrievals of daytime and nighttime profiles of several gases. For a detailed description of the satellite suite refer to Waters et al. (2006). In this paper, the version 4.2 of MLS L2 data is used for the validation. Because of the large amount of available data, tight collocation criteria are applied to find collocated measurements. The geographic distance between the centers of the two instrument footprints is required to be within 1° latitude and longitude and the time difference within 6 h. Only measurements at solar zenith angles less than 80° are considered and the difference in the modified potential vorticity at 20.5 km is required to be less than 5 PVU, in order to avoid collocation of measurements inside and outside the polar vortex. Information about potential vorticity is taken form the European Center Medium Weather Forecast (ECMWF) database (ERA interim). In case of multiple MLS collocations for the same OMPS-LP measurement, only the closest one is taken into consideration. To be consistent with NASA and sonde comparisons, MLS profiles are converted from VMR vs. pressure into number density vs. altitude (using MLS geopotential height), interpolated at the regular altitude grid of IUP-OMPS retrieved profiles and finally zonally averaged. Three latitudinal bands are selected for the comparison: 40° N - 60° N, 20° S - 20° N and 60° S - 40° S. Fig. 9 shows the averaged profiles for the tropics and relative differences in the three latitudinal bands. Standard deviations are reported in the plots as shaded areas. The number of collocations per band is in the order of 5000.

In Fig. 10, the relative differences between IUP-OMPS and MLS are shown binned in 2.5° wide latitude bins as a function of altitude. We can see here that between 20 and 50 km the differences are generally within ±10 %. An exception is the positive

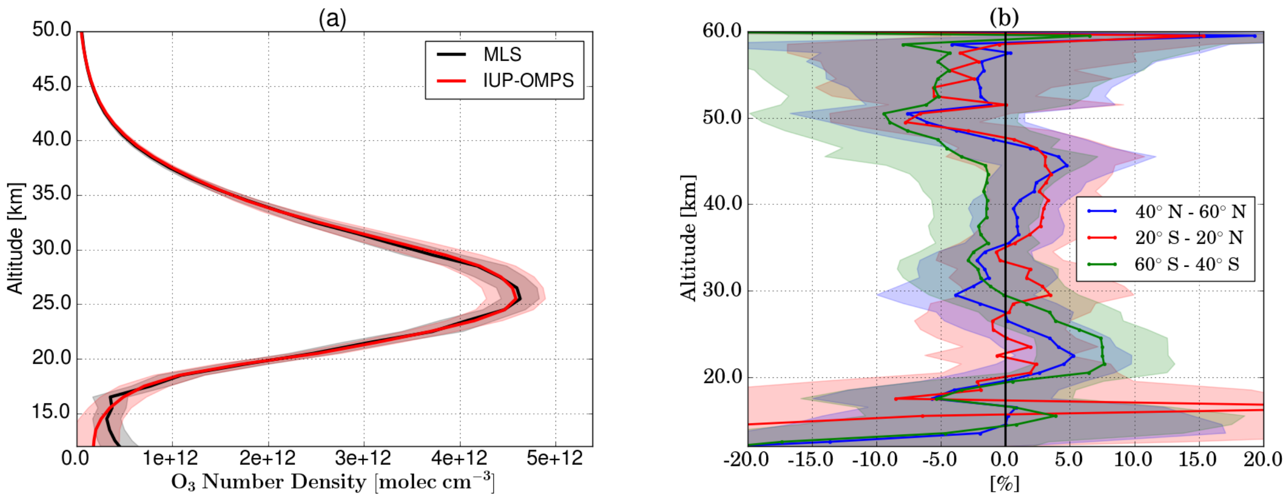

Figure 9. Panel (a): collocated IUP-OMPS retrieved profiles and MLS ozone product in the tropical region. Panel (b): relative difference profiles in the latitudinal bands 40° N - 60° N, 20° S - 20° N and 60° S - 40° S, with standard deviation shown as shaded areas.

difference (meaning that OMPS shows higher values) found in the lower tropical stratosphere, with values that locally exceed 30 %. This large discrepancy can be related to multiple factors such as the different vertical resolution of the instruments, the low sensitivity to ozone or issues with the cloud filtering. At mid-latitudes around 25 km a positive difference of 5-10 % is found. This bias can be related to the water vapor treatment inside the retrieval scheme: the intensity of the ozone number density peak is found to be sensitive to the choice of the spectral points that are skipped in the Chappuis band, where H_2O has non-negligible absorption. We also notice a significant discrepancy towards northern latitudes (> 70°) above 40 km; this disagreement can be partly related to pointing issues, due to the solar heating of the instrument at high latitudes, or stray light. A similar deviation was also found comparing IUP-OMPS and NASA retrievals at these high latitudes above 40 km (not shown). This points out possible issues in our retrieval settings, related to not screened polar mesospheric clouds, the spectral range considered in the Hartley band or to the TH normalization at 63 km. Furthermore, a dip around 50 km can be noticed, which is most probably related to the TH normalization chosen for the Huggins band, and artificial oscillations appear evident at the two uppermost levels. An increase of the smoothing parameter is expected to partially attenuate the latter problem.

5 Ozonesondes comparison

Ozonesonde data from WOUDC (World Ozone and Ultraviolet Radiation Data Center) and SHADOZ (Southern Hemisphere ADditional OZonesondes, (Thompson et al., 2007)) archives are used in this analysis. Looser collocation criteria than for MLS are selected because of the sparseness of the data set. In particular, OMPS-LP measurements are required to be within 5° in latitude and 10° in longitude from the ozonesonde station and within a 24 h time span about the sonde launch. Generally, for each sonde profile more than one OMPS-LP measurement is found using these loose criteria; therefore, all the collocated

Atmos. Meas. Tech. Discuss., https://doi.org/10.5194/amt-2017-301
Manuscript under review for journal Atmos. Meas. Tech.
Discussion started: 22 August 2017

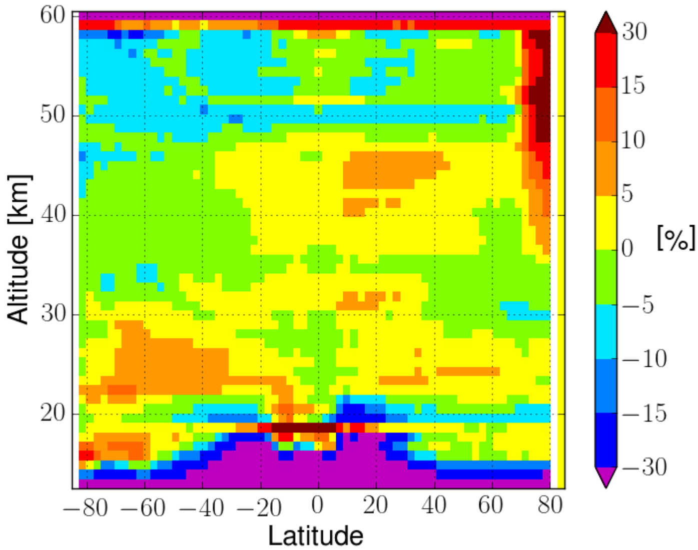

Figure 10. Relative differences between IUP-OMPS and MLS, averaged over 2.5° wide latitude bins, plotted as a function of altitude.

retrieved profiles are averaged before the comparison. Ozonesonde profiles are smoothed to the vertical resolution of the OMPS-LP retrieval grid, by using averaging kernels. For each collocated sonde profile, first the linear interpolation matrix $\mathbf{L}$ to map the low resolution OMPS profile onto the fine sonde grid is calculated and inverted using the pseudo-inverse formulation (Rodgers, 2000), obtaining $\mathbf{L}^*$ as:

$$\mathbf{L}^* = (\mathbf{L}^T\mathbf{L})^{-1}\mathbf{L}^T \tag{7}$$

Then the ozonesonde high resolution profile $\boldsymbol{x_{fine}}$ is smoothed as follows:

$$\boldsymbol{x_{coarse}} = \mathbf{A} \times \mathbf{L}^* \times \boldsymbol{x_{fine}} \tag{8}$$

The upper point of the smoothed profile is set at the OMPS-LP grid point whose respective averaging kernel altitude range is fully covered by the sonde profile. An alternative approach to this smoothing consists in a simple vertical average, considering 2.5 km ranges around each grid point (value corresponding to an average vertical resolution of the retrieval scheme, Fig. 6). The altitude where a cloud is detected by the cloud filter algorithm and all the altitudes below are screened out. Latitude bins are selected as for the previous comparisons. Averaged collocated profiles over the tropical and northern mid-latitude bands are shown in Fig. 11, with respective standard deviations. On the left side of these plots, the number of available collocations at each altitude is also reported: for tropical and northern mid-latitude bands, around 120 and 160 sonde profiles, respectively, are considered.

Fig. 12 shows the relative differences in the three latitudinal bands, in panel (a) using the averaging kernel smoothing approach and in panel (b) the vertical averaging. The lack of stations at northern and southern high latitudes prevents a meaningful

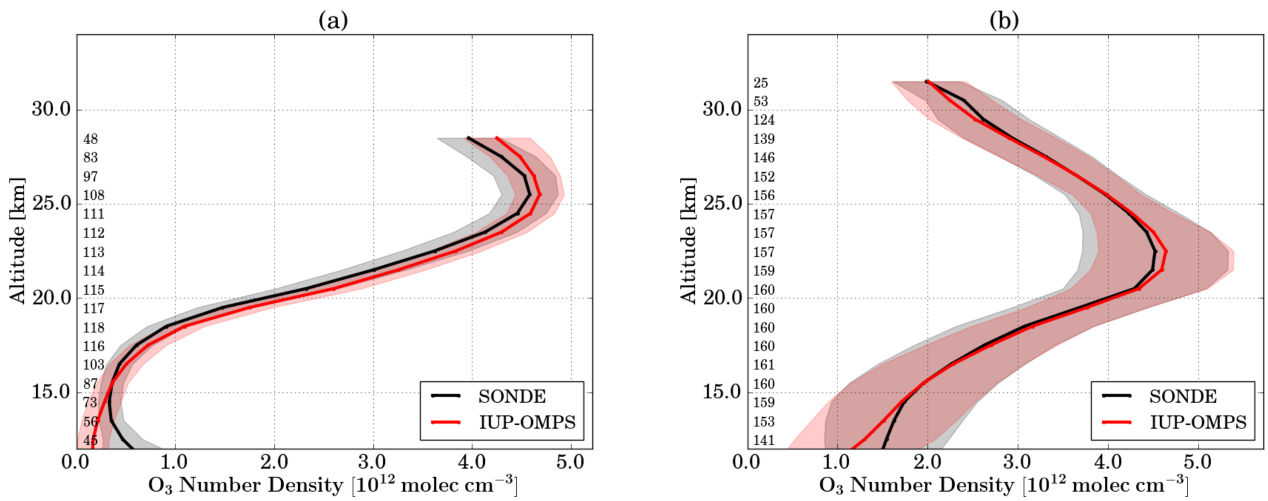

Figure 11. Comparison between collocated IUP-OMPS profiles and ozonesonde measurements in the latitudinal bands 20° S - 20° N in panel (a) and 40° N - 60° N in panel (b); standard deviations are shown as shaded areas.

comparison over this short time span. As can be seen also from Fig. 11, the agreement found at northern mid-latitudes is remarkably good, with relative differences below 5 % between 14 and 30 km. Focusing on the tropical region, a bias between the two data sets is clearly visible, with differences around 5-15 % between 20 and 32 km. This bias is unexpected considering the good agreement found when comparing to MLS data in the same region. In the lower stratosphere we also notice a peak of deviation; at these altitudes, ozone is hard to retrieve due to its decreasing concentration and the smoothing procedure may also introduce artifacts in the sonde profiles. Finally, at southern mid-latitudes, we notice a difference around 10 % between 20 and 30 km and a better agreement below. However, in this case, the validation is less significant because only two ozonesonde stations and about 25 comparisons are available over the considered time span.

With respect to the bias found in the tropical region, the processing of the OMPS-LP 2013 data set is also performed using the same retrieval settings. The analysis of these results and their validation against ozonesondes reveal a much smaller bias in the tropics. Relative differences between IUP-OMPS and sonde profiles in the same three latitudinal bands are shown in Fig. 13, following the averaging kernel smoothing approach. Since most of the sondes considered over the period Jul 2016 - Jan 2017 come from the SHADOZ archive, we also take only measurements from the same archive for the 2013 validation: over the whole year, around 140 collocations are available from 10 stations. In Fig. 13, focusing the attention on the differences in the tropical region, we can see that at least between 20 and 30 km the bias is within 5 %; larger discrepancies are still evident in the lower stratosphere. Further investigations about possible reasons for the observed behavior are ongoing.

Atmos. Meas. Tech. Discuss., https://doi.org/10.5194/amt-2017-301
Manuscript under review for journal Atmos. Meas. Tech.
Discussion started: 22 August 2017

Atmospheric Measurement Techniques
Discussions

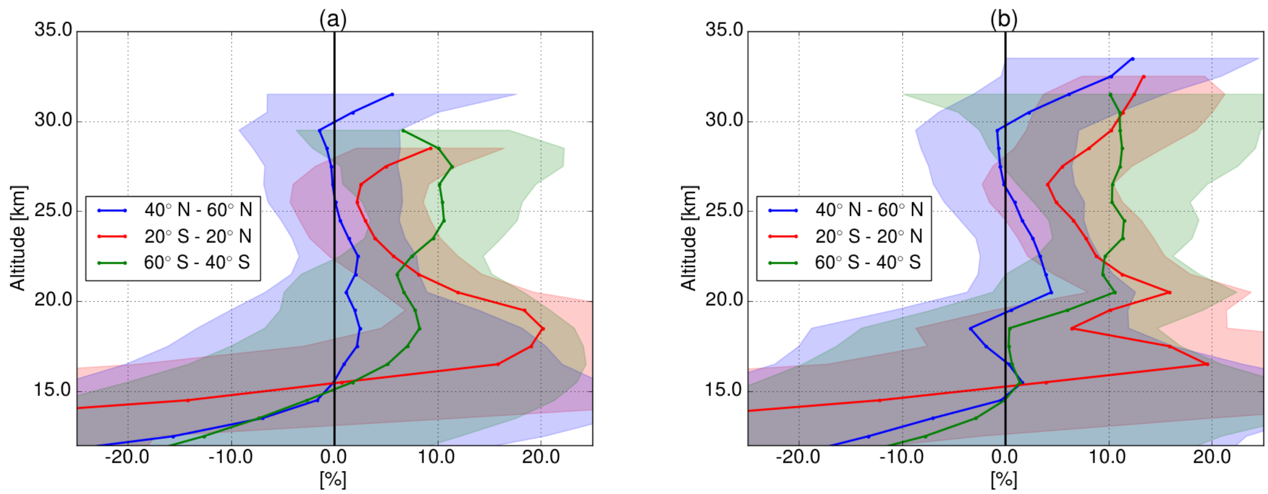

Figure 12. Relative differences between collocated IUP-OMPS profiles and ozonesonde measurements in the three latitudinal bands 40° N - 60° N, 20° S - 20° N and 60° S - 40° S, using in panel (a) averaging kernel smoothing and in panel (b) vertical averaging. Respective standard deviations are shown as shaded areas.

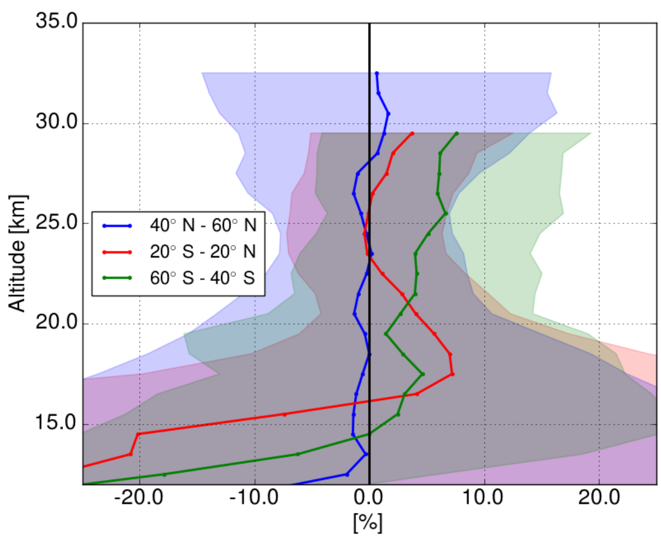

Figure 13. Relative differences between collocated IUP-OMPS profiles and ozonesonde measurements in the three latitudinal bands 40° N - 60° N, 20° S - 20° N and 60° S - 40° S for the 2013 data set, with respective standard deviations as shaded area.

6 Conclusions

The retrieval algorithm originally developed at the University of Bremen to obtain vertical distributions of ozone from SCIAMACHY limb measurements was tailored and applied to OMPS-LP observations. Seven months (Jul 2016 - Jan 2017) of v2.5 L1 gridded data were processed, analyzed and validated. Ozone profiles were retrieved between 12 and 60 km, considering only the central slit of the instrument and observations at a solar zenith angle less than 80°. A comparison with NASA v2 L2 official product was carried out, showing a general good agreement, with discrepancies within 10 % between 20 and 58 km in all considered latitude bins. The results of the validation against MLS v4.2 ozone profiles and ozonesonde measurements from SHADOZ and WOUDC archives were presented. A good agreement was found with the MLS ozone product: relative differences were generally within ±5 % between 15 and 48 km. On the other hand, a larger discrepancy between IUP-OMPS retrievals and MLS in the tropical lower stratosphere was observed, related most probably to the decreasing sensitivity of limb retrievals from both instruments in this region. A strong discrepancy above 30 % in the upper stratosphere beyond 70° N can be related to different issues: problems in the pointing of the instrument or high altitude stray light, disturbance from polar mesospheric clouds, or a sub-optimal normalization at the upper TH. In regard to the comparison with ozonesondes, at northern mid-latitudes differences within ±5 % were found between 14 and 30 km. Focusing on the tropical region, a consistent bias with SHADOZ measurements was detected, unexpected after the good agreement observed with MLS data. However, the processing and validation of the 2013 data set, using the same retrieval settings, revealed a much better agreement. The reasons for this behavior are still under investigation.

7 Data availability

Ancillary information and L2 OMPS-LP data were downloaded from https://ozoneaq.gsfc.nasa.gov/data/omps/, where v2.5 L1 gridded data are now also available.
For the validation sections, MLS L2 data were taken from https://disc.gsfc.nasa.gov/datasets. WOUDC data were retrieved on May 18, 2017, from http://woudc.org; a list of all contributors is available on the following website: doi:10.14287/10000001. SHADOZ were retrieved on April 6, 2017 from https://tropo.gsfc.nasa.gov/shadoz/Archive.html. Our results are available upon request to the University of Bremen.

Author contributions. CA adapted the retrieval algorithm to OMPS-LP observations, processed the data set, performed the validation of the results and wrote the manuscript. AR provided the retrieval algorithm exploited in this study, supervised and guided the retrieval process and reviewed the paper. EM provided retrieved aerosol extinction profiles. K-UE contributed with the algorithm for cloud filtering that was adapted to OMPS-LP observations. TvC contributed to the discussion of the regularization matrices for the retrieval scheme and the proper use of averaging kernels to smooth the ozonesonde profiles and reviewed the paper. JPB is the main leader of the project, discussed and reviewed the paper.

Competing interests. The authors declare that they have no conflict of interests. TvC is associated editor of AMT but is not involved in the reviewing of this particular paper.

Acknowledgements. This work was partially funded by ESA within the Ozone CCI project and was supported by the University and State of Bremen. We would like to acknowledge NASA OMPS SIPS team (in particular G. Jaross, N. Kramarova and P.K. Bhartia) for the support provided during the data analysis as well as for the concession of the new v2.5 of OMPS-LP L1 data before its official release.

References

Aschmann, J., Burrows, J. P., Gebhardt, C., Rozanov, A., Hommel, R., Weber, M., and Thompson, A. M.: On the hiatus in the acceleration of tropical upwelling since the beginning of the 21st century, Atmospheric Chemistry and Physics, 14, 12 803–12 814, doi:10.5194/acp-14-12803-2014, http://www.atmos-chem-phys.net/14/12803/2014/, 2014.

Bhartia, P., Jaross, G., Larsen, J., and Fleig, A.: Science Team Evaluation of the OMPS Limb Profiler, Tech. rep., 2013.

Bogumil, K., Orphal, J., Burrows, J. P., et al.: Temperature dependent absorption cross sections of O3, NO2, and other atmospheric trace gases measured with the SCIAMACHY spectrometer, in: Proceedings of the ERS-Envisat-Symposium, Goteborg, Sweden, 2000.

Burrows, J., Hölzle, E., Goede, A., Visser, H., and Fricke, W.: SCIAMACHY—Scanning imaging absorption spectrometer for atmospheric chartography, Acta Astronautica, 35, 445–451, 1995.

Eckert, E., Clarmann, T. v., Kiefer, M., Stiller, G., Lossow, S., Glatthor, N., Degenstein, D., Froidevaux, L., Godin-Beekmann, S., Leblanc, T., et al.: Drift-corrected trends and periodic variations in MIPAS IMK/IAA ozone measurements, Atmospheric Chemistry and Physics, 14, 2571–2589, 2014.

Eichmann, K.-U., Lelli, L., von Savigny, C., Sembhi, H., and Burrows, J. P.: Global cloud top height retrieval using SCIAMACHY limb spectra: model studies and first results, Atmospheric Measurement Techniques, 9, 793–815, doi:10.5194/amt-9-793-2016, https://www.atmos-meas-tech.net/9/793/2016/, 2016.

Farman, J. C., Gardiner, B. G., and Shanklin, J. D.: Large losses of total ozone in Antarctica reveal seasonal ClOx/NOx interaction, Nature, 315, 207–210, 1985.

Flynn, L., Long, C., Wu, X., Evans, R., Beck, C., Petropavlovskikh, I., McConville, G., Yu, W., Zhang, Z., Niu, J., et al.: Performance of the ozone mapping and profiler suite (OMPS) products, Journal of Geophysical Research: Atmospheres, 119, 6181–6195, 2014.

Gebhardt, C., Rozanov, A., Hommel, R., Weber, M., Bovensmann, H., Burrows, J., Degenstein, D., Froidevaux, L., and Thompson, A.: Stratospheric ozone trends and variability as seen by SCIAMACHY from 2002 to 2012, Atmospheric Chemistry and Physics, 14, 831–846, 2014.

Gottwald, M. and Bovensmann, H.: SCIAMACHY-Exploring the changing Earth's Atmosphere, Springer Science & Business Media, 2011.

Hartley, W.: On the probable absorption of solar radiation by atmospheric ozone, Chem News, 42, 1880.

Hassler, B., Petropavlovskikh, I., Staehelin, J., August, T., Bhartia, P., Clerbaux, C., Degenstein, D., Mazière, M. D., Dinelli, B., Dudhia, A., et al.: Past Changes in the Vertical Distribution of Ozone Part 1: Measurement Techniques, Uncertainties and Availability, 2014.

Hess, M., Koepke, P., and Schult, I.: Optical properties of aerosols and clouds: The software package OPAC, Bulletin of the American meteorological society, 79, 831–844, 1998.

Jaross, G., Bhartia, P. K., Chen, G., Kowitt, M., Haken, M., Chen, Z., Xu, P., Warner, J., and Kelly, T.: OMPS Limb Profiler instrument performance assessment, Journal of Geophysical Research: Atmospheres, 119, 4399–4412, 2014.

Jia, J., Rozanov, A., Ladstätter-Weißenmayer, A., and Burrows, J.: Global validation of SCIAMACHY limb ozone data (versions 2.9 and 3.0, IUP Bremen) using ozonesonde measurements, Atmospheric Measurement Techniques, 8, 3369–3383, 2015.

Kahn, D. and Kowitt, M.: Limb Gridded Radiance User Guide, LP-L1G-EV-1.0, version 2.0, Tech. rep., 2015.

Kyrölä, E., Laine, M., Sofieva, V., Tamminen, J., Päivärinta, S.-M., Tukiainen, S., Zawodny, J., and Thomason, L.: Combined SAGE II–GOMOS ozone profile data set for 1984–2011 and trend analysis of the vertical distribution of ozone, Atmospheric Chemistry and Physics, 13, 10 645–10 658, 2013.

Manney, G. L., Santee, M. L., Rex, M., Livesey, N. J., Pitts, M. C., Veefkind, P., Nash, E. R., Wohltmann, I., Lehmann, R., Froidevaux, L., et al.: Unprecedented Arctic ozone loss in 2011, Nature, 478, 469–475, 2011.

Molina, M. J. and Rowland, F. S.: Stratospheric sink for chlorofluoromethanes: chlorine atom-catalysed destruction of ozone, Nature, 249, 810–812, 1974.

Moy, L., Bhartia, P. K., Jaross, G., Loughman, R., Kramarova, N., Chen, Z., Taha, G., Chen, G., and Xu, P.: Altitude registration of limb-scattered radiation, Atmospheric Measurement Techniques, 10, 167–178, 2017.

Nedoluha, G., Siskind, D., Lambert, A., and Boone, C.: The decrease in mid-stratospheric tropical ozone since 1991, Atmospheric Chemistry and Physics, 15, 4215–4224, 2015.

Pachauri, R. and Meyer, L.: IPCC, 2014: Climate Change 2014: Synthesis Report. Contribution of Working Groups I, II and III to the Fifth Assessment Report of the Intergovernmental Panel on Climate Change, 2014.

Rault, D. F. and Loughman, R. P.: The OMPS Limb Profiler environmental data record algorithm theoretical basis document and expected performance, IEEE Transactions on Geoscience and Remote Sensing, 51, 2505–2527, 2013.

Rieger, L., Malinina, E., Rozanov, A., Burrows, J. P., Bourassa, A., and Degenstein, D.: Error Estimation for Limb Scatter Aerosol Extinction Retrievals Using OSIRIS and SCIAMACHY, to be submitted to Atmos. Meas. Tech. by the end of autumn, 2017.

Rodgers, C. D.: Inverse methods for atmospheric sounding: theory and practice, vol. 2, World scientific, 2000.

Rozanov, A., Weigel, K., Bovensmann, H., Dhomse, S., Eichmann, K.-U., Kivi, R., Rozanov, V., Vömel, H., Weber, M., and Burrows, J.: Retrieval of water vapor vertical distributions in the upper troposphere and the lower stratosphere from SCIAMACHY limb measurements, Atmospheric Measurement Techniques, 4, 933–954, 2011.

Rozanov, A. V., Rozanov, V. V., and Burrows, J. P.: Combined differential-integral approach for the radiation field computation in a spherical shell atmosphere: Nonlimb geometry, Journal of Geophysical Research: Atmospheres, 105, 22 937–22 942, 2000.

Rozanov, V., Rozanov, A., Kokhanovsky, A., and Burrows, J.: Radiative transfer through terrestrial atmosphere and ocean: software package SCIATRAN, Journal of Quantitative Spectroscopy and Radiative Transfer, 133, 13–71, 2014.

Serdyuchenko, A., Gorshelev, V., Weber, M., Chehade, W., and Burrows, J. P.: High spectral resolution ozone absorption cross-sections – Part 2: Temperature dependence , Atmospheric Measurement Techniques, 7, 625–636, doi:10.5194/amt-7-625-2014, https://www.atmos-meas-tech.net/7/625/2014/, 2014.

Sofieva, V. F., Kyrölä, E., Laine, M., Tamminen, J., Degenstein, D., Bourassa, A., Roth, C., Zawada, D., Weber, M., Rozanov, A., Rahpoe, N., Stiller, G., Laeng, A., von Clarmann, T., Walker, K. A., Sheese, P., Hubert, D., van Roozendael, M., Zehner, C., Damadeo, R., Zawodny, J., Kramarova, N., and Bhartia, P. K.: Merged SAGE II, Ozone_cci and OMPS ozone profiles dataset and evaluation of ozone trends in the stratosphere, Atmospheric Chemistry and Physics Discussions, 2017, 1–28, doi:10.5194/acp-2017-598, https://www.atmos-chem-phys-discuss.net/acp-2017-598/, 2017.

Solomon, S., Ivy, D. J., Kinnison, D., Mills, M. J., Neely, R. R., and Schmidt, A.: Emergence of healing in the Antarctic ozone layer, Science, 353, 269–274, 2016.

Steinbrecht, W., Froidevaux, L., Fuller, R., Wang, R., Anderson, J., Roth, C., Bourassa, A., Degenstein, D., Damadeo, R., Zawodny, J., et al.: An update on ozone profile trends for the period 2000 to 2016 [Discussions paper], 2017.

Stiller, G. P., Fierli, F., Ploeger, F., Cagnazzo, C., Funke, B., Haenel, F. J., Reddmann, T., Riese, M., and von Clarmann, T.: Shift of subtropical transport barriers explains observed hemispheric asymmetry of decadal trends of age of air, Atmospheric Chemistry and Physics Discussions, 2017, 1–16, doi:10.5194/acp-2016-1162, https://www.atmos-chem-phys-discuss.net/acp-2016-1162/, 2017.

Stolarski, R. and Frith, S.: Search for evidence of trend slow-down in the long-term TOMS/SBUV total ozone data record: the importance of instrument drift uncertainty, Atmospheric Chemistry and Physics, 6, 4057–4065, 2006.

Thompson, A. M., Witte, J. C., Smit, H. G., Oltmans, S. J., Johnson, B. J., Kirchhoff, V. W., and Schmidlin, F. J.: Southern Hemisphere Additional Ozonesondes (SHADOZ) 1998–2004 tropical ozone climatology: 3. Instrumentation, station-to-station variability, and evaluation with simulated flight profiles, Journal of Geophysical Research: Atmospheres, 112, 2007.

Tikhonov, A. N.: Solution of incorrectly formulated problems and the regularization method, Soviet Math. Dokl., 4, 1035–1038, 1963.

Waters, J. W., Froidevaux, L., Harwood, R. S., Jarnot, R. F., Pickett, H. M., Read, W. G., Siegel, P. H., Cofield, R. E., Filipiak, M. J., Flower, D. A., et al.: The earth observing system microwave limb sounder (EOS MLS) on the Aura satellite, IEEE Transactions on Geoscience and Remote Sensing, 44, 1075–1092, 2006.

WMO: Scientific Assessment of Ozone Depletion 2014, Global Ozone Research and Monitoring Project Report 55, World Meterological Organization, https://www.esrl.noaa.gov/csd/assessments/ozone/2014/chapters/\2014OzoneAssessment.pdf, 2014.